

# Robot design of underwater building surface dredging -- structural design

---

## ABSTRACT

In order to improve the efficiency of dredging, reduce the cost of dredging and ensure the safety of operation, this paper designs an underwater building surface dredging robot (hereinafter referred to as "underwater dredging robot"), which mainly includes the following aspects. The structure of underwater dredging robot is planned and divided into dredging system, walking system, driving system and support system. According to the actual work situation and the characteristics of each system, the scheme selection and structure design are carried out, and the overall layout scheme is obtained. The materials of the support system are selected and its force under different working conditions is analyzed. Through finite element analysis and modal analysis, it is verified that its reliability meets the requirements and there is no resonance phenomenon in the work.

*Keywords:* **Dredging robot; Structural design; Statics; Modal; ANSYS.**

## 1. INTRODUCTION

Underwater dredging robot is a new means of solving the problem of silt deposition, which can avoid the shortcomings of traditional dredging methods through autonomous control and flexibility[1]. The core component of the robot is the dredging head, which sucks the silt into the dredging pipe through rotation and high-pressure water flow, and sends it to the designated treatment site. The robot has the advantages of high efficiency, low cost, and low ecological impact[2].

The types of underwater robots include both manned underwater robots (HOV) and unmanned underwater robots (UUV)[3]. Among them, unmanned underwater robots can be further divided into three categories: autonomous underwater robots (AUVs), cable-controlled underwater robots (ROVs), and autonomous and cable-controlled composite underwater robots (ARVs)[4]. Considering the safety of the staff, the underwater dredging robot should not carry people when dredging, so the manned underwater robot is not considered[5]. In the unmanned underwater robots, autonomous underwater robots and autonomous and cable-controlled composite underwater robots are involved in the cable-free design, so they have a high R & D technology requirements, high cost and the use of high risk and a number of unfavorable factors for R & D. The cable-controlled underwater robot is not only the most powerful underwater robot, but also the most powerful underwater robot. The cable-controlled underwater robot can not only avoid the above unfavorable factors, but also has the advantages of small and flexible, easy to control, easy to maintain, and controllable work intensity. Therefore, the underwater building surface dredging robot designed in this paper will draw on the cable-controlled underwater robot technology program[6].

In this paper, by comparing the advantages and disadvantages of different working methods of each system, we have selected the appropriate working method and structural design for underwater dredging. And the key system parameters are calculated and selected, and the mechanical properties of the key structure will be analyzed in depth[7].

## 2. STRENGTH ANALYSIS OF LOAD-BEARING BRACKET FOR UNDERWATER DREDGING ROBOT

### 2.1 STRENGTH ANALYSIS OF UNDERWATER DREDGING ROBOT LOAD-BEARING BRACKET DESIGN OF BRACKET SYSTEM

The bracket system consists of three parts: the carrier bracket, the chassis bracket and the connection bracket[8]. Considering that the metal is easily corroded by the underwater working environment, the material of the carrier bracket adopts alloy steel, while the material of the chassis bracket and the connecting bracket adopts stainless steel[9]. In order to meet the requirements of different working conditions, the bracket can be adjusted according to the actual situation to ensure that the overall performance is optimized. The structure of the chassis bracket is shown in Figure 1, the bottom beam of the submersible pump support and the bottom beam of the load-bearing bracket are firmly fixed on the chassis.

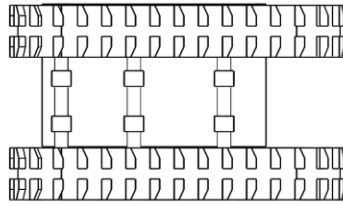


**Fig. 1. The structure of the chassis bracket**

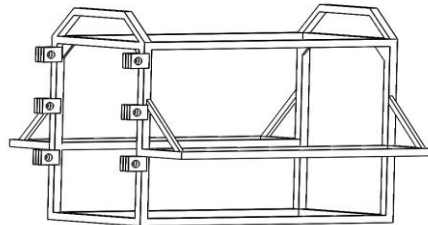


**Fig. 2. The structure of the bearing bracket**

The structure of the carrier bracket is shown in Figure 2. The support structure of the robot consists of two hydraulic cylinder supports and four connecting frame supports, while the hood mount is located at one end of the carrier bracket[10]. In order to ensure the reliability of the structure, diagonal plates and diagonal ribs were added to support the carrier brackets.

As shown in Fig. 3, the connecting brackets are constructed in the form of long tubes, one end of which is used to hold the winch and the other end is used to connect the hydraulic cylinders. Two mounting holes are provided at each end of the bracket for interconnecting the winch section and the carrier bracket. The hydraulic cylinder connector is provided in the middle of the bracket to which the hydraulic cylinder is attached to facilitate installation of the hydraulic cylinder[11].

The overall arrangement of the underwater dredging robot is shown in FIG. 4, wherein from left to right and from top to bottom, there are a dredging system, a carrier system, a drive system, and a traveling system, in that order. Among them, the dredging system consists of a winch, a winch motor, a winch cover, a winch motor cover, and a suction pipe and a submersible pump[12]. The dredging system is connected to the carrier bracket through the connecting bracket, and the hydraulic cylinders are connected to the carrier bracket by the top two connecting brackets to complete the lifting and lowering of the winch system. The center part of the winch cover has a circular opening with a fence structure at the circular opening, and is connected to the submersible pump through a sewage pipe to complete the silt transportation work.

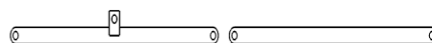


**Fig. 3 Connecting bracket structure**

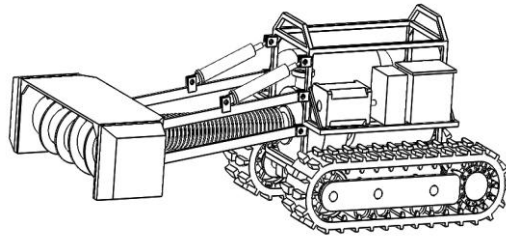


**Fig. 4 Overall layout of underwater dredging robot**

## 2.2 STRENGTH ANALYSIS OF THE LOAD-BEARING BRACKET

The material of the bracket is alloy steel, which is a plastic material with a density of  $7.70\text{g/cm}^3$ , a modulus of elasticity of  $210\text{GPa}$ , and a Poisson's ratio of  $0.28$ . The tensile strength of the stainless steel material is  $723.82\text{MPa}$ , and the yield strength is  $620.42\text{MPa}$ .

The three-dimensional model of the load-bearing bracket is processed, its geometry is simplified, the material is set, and then the structure is divided into grids, the cell size is set to  $24\text{mm}$ , and finally a total of  $9158$  cells are obtained, and the grid is divided as shown in Figure 5.

Due to the different positions and states of the stringer dredging system, the force of the load-bearing bracket also changes. For the position of the winch dredging system, two limit positions are analyzed, i.e. lifting and lowering, while the state of the winch dredging system is divided into two working states, i.e. the winch is stationary and the winch is moving at a uniform speed. When the winch operates at a maximum speed at constant velocity, the perpendicular distance between the center of mass of the rotating part and the axis of rotation is called the eccentricity distance, which is  $3.35\text{mm}$ . At this time, the angular velocity is  $5.23\text{rad/s}$ , and the inertial principal vector of the center of rotation is  $14.67\text{N}$ , while the inertial principal moment is  $0$ . The analysis of the overall force shows that, because the rotating part of the rotating part is symmetrical about the middle of the axis, the forces along the axial direction cancel each other out, and only the resistance force along the tangential direction exists. Resistance exists only along the tangential direction. However, this resistance is less than the maximum equivalent force of  $262.5\text{N}$ , so a load factor of  $1.8$  is used to calculate the total resistance for safety reasons. Therefore, the magnitude of the resistance force is  $500\text{N}$  in the direction opposite to the direction of rotation.

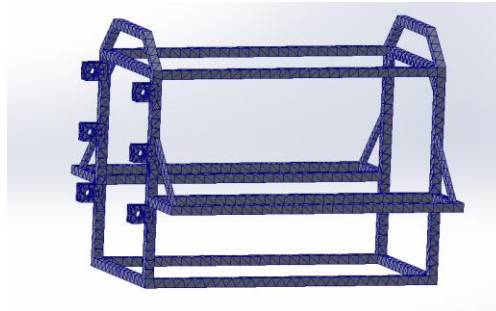


**Fig. 5 Carrier bracket grid division model**

### 2.2.1 THE WINCH IS STATIONARY AND IN THE UPPER LIMIT POSITION

The force on one side of the connecting bracket structure has been shown in Fig. 4.2,  $F_1$  is the tension force of the carrier bracket on the hydraulic cylinder,  $F_2$  and  $F_3$  are the support force of the carrier bracket on the connecting bracket, and  $F_4$  is half of the gravity force of the stringer part.

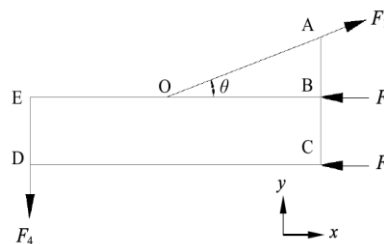


**Fig. 6 Working condition 1: Force on connecting support**

Balance equation for the whole structure:

$$\begin{cases} \sum F_x = 0 \\ \sum F_y = 0 \\ \sum M_o(F) = 0 \end{cases} \Rightarrow \begin{cases} F_1 \cdot \cos \theta - F_2 - F_3 = 0 \\ F_1 \cdot \sin \theta - F_4 = 0 \\ F_4 \cdot L_{OE} - F_3 \cdot L_{BC} = 0 \end{cases} \quad (1)$$

According to the design data of the bracket system, we can get  $\tan\theta=16/45$ ,  $F_4=1715\text{N}$ , after calculation, we can get  $F_1=5118.8\text{N}$ ,  $F_2=1012\text{N}$ ,  $F_3=3811\text{N}$ . According to the axiom of two-force equilibrium, we can get the force that the load-bearing bracket suffers in the connection is equal in magnitude and opposite in direction to the above force. The constraint is applied to the load-bearing bracket and the simulation calculation of equivalent stress and total deformation is carried out, and the stress cloud diagram and deformation cloud diagram are obtained as shown in Figure 7.

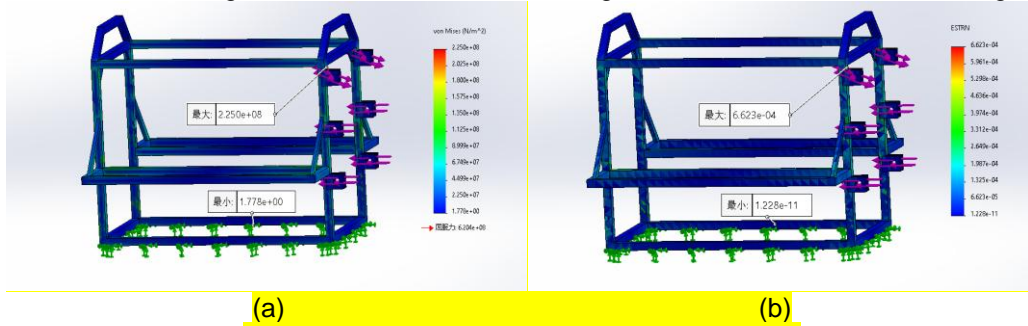


Fig. 7 Simulation results of working condition 1

### 2.2.2 THE WINCH IS STATIONARY AND IN THE LOWER LIMIT POSITION

The force on one side of the connecting bracket structure has been shown in Fig. 8,  $F_1$  is the tension force of the carrier bracket on the hydraulic cylinder,  $F_2$  and  $F_3$  are the support force of the carrier bracket on the connecting bracket, and  $F_4$  is half of the gravity force of the winch part in the dredging system. From the design data of the bracket system, we get  $\angle OAB = 45.3^\circ$ .

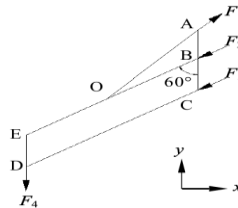


Fig. 8 Working condition 2: Force of connecting bracket

Balance equations are presented for the entire structure:

$$\begin{cases} \sum F_x = 0 \\ \sum F_y = 0 \\ \sum M_A(F) = 0 \end{cases} \Rightarrow (2)$$

$$\begin{cases} F_1 \cdot \sin 45.3^\circ - F_2 \cdot \sin 60^\circ - F_3 \cdot \sin 60^\circ = 0 \\ F_1 \cdot \cos 45.3^\circ - F_4 - F_2 \cdot \cos 60^\circ - F_3 \cdot \cos 60^\circ = 0 \\ F_4 \cdot L_{CD} \sin 60^\circ - F_3 \sin 60^\circ \cdot L_{AC} - F_2 \sin 60^\circ \cdot L_{AB} = 0 \end{cases} \quad (3)$$

Calculated  $F_1=5737.5\text{N}$ ,  $F_2=520.58\text{N}$ ,  $F_3=4163.9\text{N}$ . According to the axiom of two-force equilibrium to apply constraints on the load-bearing bracket, the stress cloud and deformation cloud are obtained as shown in Fig. 9

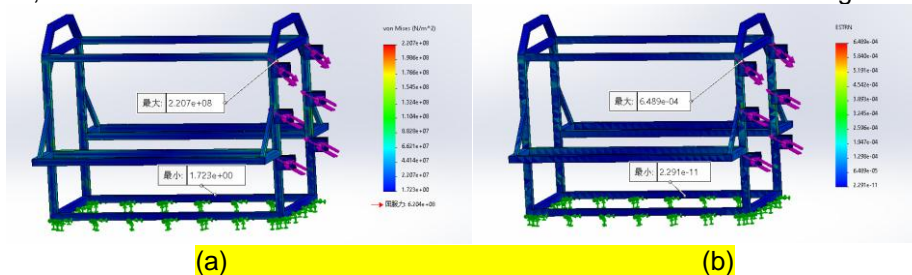
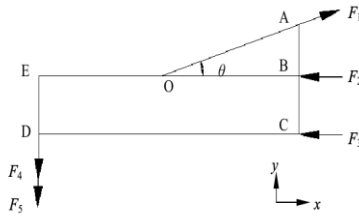


Fig. 9 Condition 2 equivalent force cloud diagram

### 2.2.3 WINCH WORKING AND IN THE UPPER LIMIT POSITION

The force on one side of the connecting bracket structure has been shown in the figure,  $F_1$  is the tension force of the carrier bracket on the hydraulic cylinder,  $F_2$ ,  $F_3$  is the support force of the carrier bracket on the connecting bracket,  $F_4$  is half of the gravity force of the gibbet portion of the gibbet,  $F_5=250\text{N}$ , is the resistance force.



**Fig. 10 Working condition 3: Force of connecting bracket**

Balance equations are presented for the entire structure:

$$\begin{cases} \sum F_x = 0 \\ \sum F_y = 0 \\ \sum M_o (F) = 0 \end{cases} \Rightarrow \begin{cases} F_1 \cdot \cos \theta - F_2 - F_3 = 0 \\ F_1 \cdot \sin \theta - F_4 - F_5 = 0 \\ (F_4 + F_5) \cdot L_{OE} - F_3 \cdot L_{BC} = 0 \end{cases} \quad (4)$$

The calculated  $F_1$  is 5866 N,  $F_2$  is 1160 N, and  $F_3$  is 4367 N. According to the axiom of two-force equilibrium to apply constraints on the load-bearing bracket, the stress and deformation clouds are obtained as shown in Fig. 11.

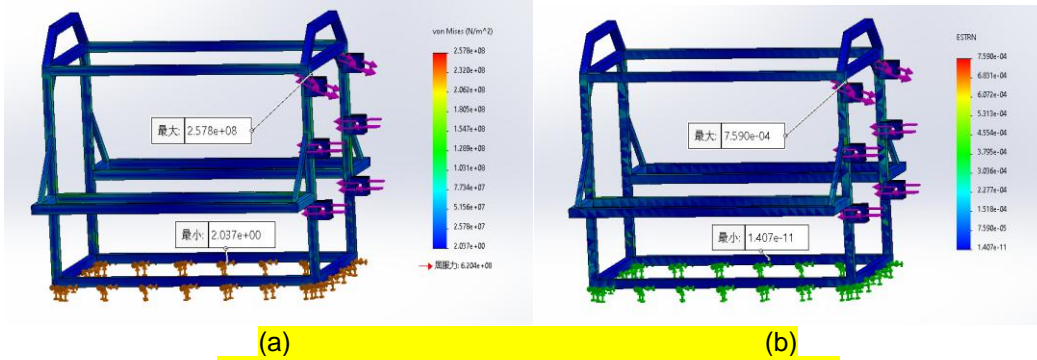


**Fig. 11 Simulation results of working condition 3**

## 2.2.4 THE WINCH IS WORKING AND IN THE LOWER LIMIT POSITION

The force on one side of the connecting bracket structure is shown in Fig.  $F_1$  is the tension force of the carrying bracket on the hydraulic cylinder,  $F_2$  and  $F_3$  are the support force of the carrying bracket on the connecting bracket,  $F_4$  is half of the gravity force of the winch portion, and  $F_5=250\text{N}$ , which is the resistance force.

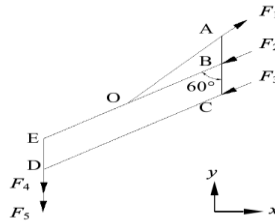


**Fig. 12 Working condition 4: Force of connecting bracket**

Balance equations are presented for the entire structure:

$$\begin{cases} \sum F_x = 0 \\ \sum F_y = 0 \\ \sum M_A (F) = 0 \end{cases} \Rightarrow (5)$$

$$\begin{cases} F_1 \cdot \sin 45.3^\circ - F_2 \cdot \sin 60^\circ - F_3 \cdot \sin 60^\circ = 0 \\ F_1 \cdot \cos 45.3^\circ - F_4 - F_5 - F_2 \cdot \cos 60^\circ - F_3 \cdot \cos 60^\circ = 0 \\ (F_4 + F_5) \cdot L_{CD} \sin 60^\circ - F_3 \sin 60^\circ \cdot L_{AC} - F_2 \sin 60^\circ \cdot L_{AB} = 0 \end{cases} \quad (6)$$

According to the design data of the bracket system,  $F_1$  is calculated to be 6576.27N,  $F_2$  is 863.25N, and  $F_3$  is 4505.6N.

According to the two-force equilibrium axiom to impose constraints on the load-bearing bracket, and simulation calculations of equivalent stress and total deformation were carried out, and the stress cloud and deformation cloud were obtained as shown in Fig. 13.

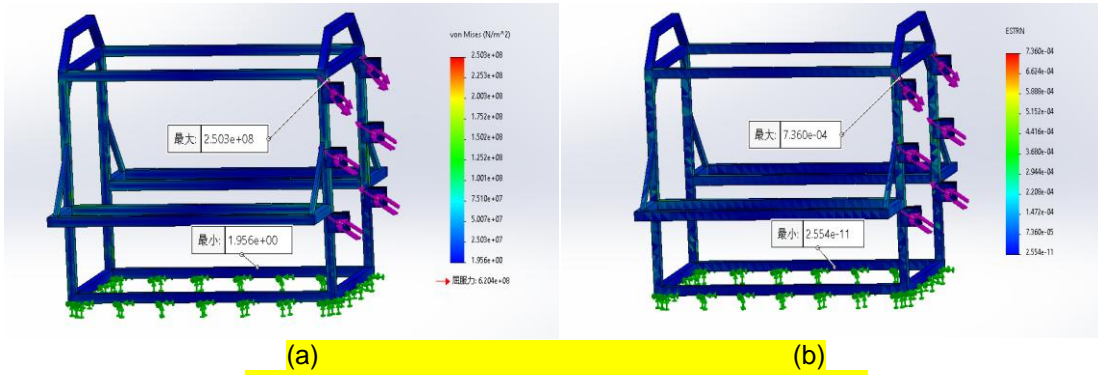


**Fig. 13 Simulation results of working condition 3**

A comprehensive summary of the maximum stresses and deformations sustained by the load-bearing brackets under different operating conditions is shown in Table 1.

**Table 1 Data processing under various operating conditions**

Working condition category	Maximum stress/MPa	Maximum deformation/mm
1	225	0.66
2	220.7	0.65
3	257.8	0.76
4	250.3	0.74

After analyzing the load bearing bracket under different working conditions, it is found that the maximum stress and maximum deformation will reach the maximum value when the winch is in motion and in the lowered position. The maximum stress of the load-bearing support is 257.8MPa, which is less than the yield strength of the material, and the maximum deformation is 0.76mm, which is also within the tolerable range.

### 3.MODAL ANALYSIS OF LOAD-BEARING BRACKETS

Modal Analysis (MA) is a method used to study the free vibration characteristics inherent in an object during vibration. Modal analysis can be carried out through the following steps: first, collect the information of the structure's geometry and material parameters to establish a mathematical model; then, solve the eigenvalues and eigenvectors of the structure to obtain the information of the structure's natural frequency, damping ratio, and vibration mode, etc.; finally, based on the information, evaluate the response characteristics of the structure, such as the amplitude, displacement, acceleration, etc., as well as the existence of the phenomenon of resonance, and carry out the structural optimized design to meet the design requirements. Through these measures, resonance phenomenon can be effectively avoided during the use of the structure, and the safety and reliability of the structure can be improved.

Define the material, mesh and constraints on the load-bearing bracket model, add fixed constraints on the bottom surface of the load-bearing bracket, and add forces on each stress surface, and set the conditions the same as those in the static analysis. The first-order modes of its four operating states are analyzed, resulting in Fig. 14.

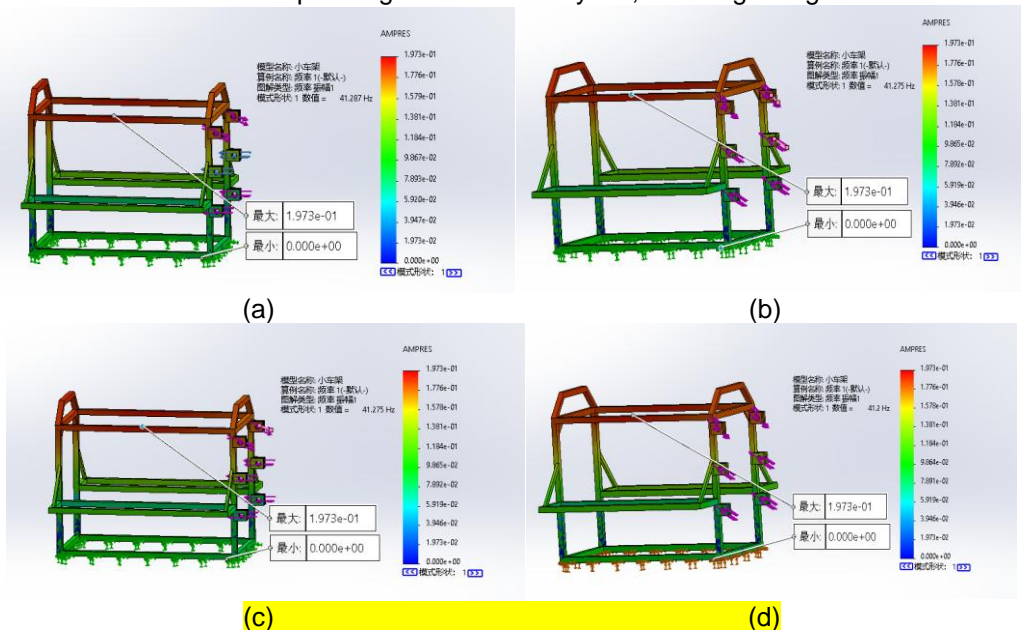


**Fig. 14 Modal analysis results**

**Table 2 Natural frequency of bearing bracket**

working condition	1	2	3	4
Intrinsic frequency/Hz	41.29	41.28	41.28	41.2

The intrinsic frequencies of the modes for each working condition are shown in Table 2. According to the results of modal analysis, under different working conditions of the underwater dredging robot, the first modal frequency of the load carrier ranges from 41.2 Hz to 41.29 Hz, compared with the vibration frequency range of 0-20 Hz generated by the traveling system, the vibration frequency caused by the transmission imbalance ranges from 6-15 Hz, and the vibration frequency generated by the drive motor is 5.2 Hz. Due to the fact that the excitation frequency range is much smaller than the intrinsic frequency of the load carrier, it can be ensured that the intrinsic frequency of the load carrier will not resonate with the above excitations, thus satisfying the requirement of the intrinsic frequency. range is much smaller than the intrinsic frequency of the load-bearing bracket, so it can ensure that the intrinsic frequency of the load-bearing bracket will not resonate with the above excitation, thus meeting the requirements of the structural design.

#### 4.SUMMARY

In this paper, a modernized dredging method, i.e., the use of an underwater dredging robot to quickly and efficiently clean silt, is proposed as an alternative to the traditional method. The structural design of the robot was verified to be reasonable after mechanical performance analysis, and the underwater dredging robot bracket system was designed. After material screening and mechanical analysis, the stresses of the load-bearing bracket under different working conditions were studied in depth, and finite element analysis technology was used to derive the maximum stresses and deformations borne by the structure under the corresponding working conditions to ensure its reliability. After modal analysis, the intrinsic frequency of the load-bearing bracket is studied in depth to ensure that there will not be any resonance phenomenon when it is working.

#### COMPETING INTERESTS

Authors have declared that no competing interests exist.

#### AUTHORS' CONTRIBUTIONS

This work was carried out in collaboration among all authors. All authors read and approved the final manuscript.

#### REFERENCES

1. Dang Hongxing. Mechanism design and gait research of bionic turtle underwater dredging robot [D]. Harbin Engineering University, 2021.
2. Gao Shengbiao. Structural design and control system research of underwater dredging robot[D]. Hunan University,2020.
3. Lu J ,Zhu D .Design of city sewer dredging robot with variable diameter[J].Journal of Physics: Conference Series,2018,1074(1).
4. Jiman Luo,SiyuanLiu,Lulu Dai et al. Design and dynamic characterization of pipeline robot dredging device[J]. machinery and electronics,2018,36(08).
5. ZHAO Hui,LIJintao,WANG Fei et al. Design of anti seepage canal dredging robot in South Xinjiang region[J]. Xinjiang Agricultural Mechanization,2022,(01).
6. Zhang Chao. Research on pipeline dredging robot[D]. Shijiazhuang Railway University,2019.
7. Ding YW. Design and development of medium-sized nuclear pipeline inspection and dredging robot[D]. Tianjin University,2021.
8. Ao R. Structural design and performance analysis of a parallel pipeline dredging robot with adjustable diameter [D]. Yanshan University, 2021.
9. Yin Hui. Research on adaptive control of dredging robot based on electromechanical joint simulation[D]. Shenyang University of Architecture, 2021.
10. Zi Zhuo. Development of pipeline dredging robot and its mixing and conveying characteristics [D]. Beijing Jiaotong University, 2022.
11. Liu S-Y. Research on optimized design and dynamic characteristics of pipeline robot dredging device[D]. Shenyang University of Architecture,2019.
12. Li Aimin,YuHu,LiYunpeng et al. Design of pipeline dredging robot[J]. Light Industry Science and Technology,2019,35(03).

13. MARTIN S C, WHITCOMB L L. FULLY Actuated Model-Based Control with Six-Degree-of-Freedom Coupled Dynamical Plant Models for Underwater Vehicles: Theory and Ex-Per imental Evaluation[J]. International Journal of Robotics Research, 2016, 35(10):1164-1184.
14. Yang Shengmei, Zhao Qiuyun. Current status of the application of underwater robots[J]. Water Resources and Hydropower Express, 2015, 36(11):29-31.